Guest Editorial Special Issue on Verification and Validation of Air Gun Source Signature and Sound Propagation Models

THIS special issue of the IEEE JOURNAL OF OCEANIC ENGINEERING focuses on the verification and validation of models for predicting the sound field radiated by air guns and air gun arrays. The special issue aims to address the demand for increasingly precise assessments of environmental impacts, requiring accurate characterization of the air gun array sound field, including the interface between source signature models and sound propagation models. To address this need, a modeling workshop was held in July 2016. Participants in the 2016 workshop were asked to predict, for specified scenarios, the time series of sound pressure and sound particle acceleration at different positions relative to the source, as well as the source waveform. Air gun modeling experts worldwide, including the 2016 workshop participants, were invited to contribute to this special issue. The first paper in the special issue describes the 2016 workshop and its main findings and the second paper describes the test scenarios. The remaining papers, most of which present results for the test scenarios, describe either source waveforms, or sound pressure or particle acceleration time series, or both. This editorial summarizes all papers in the special issue, paying special attention to comparing different participants' results for the same test scenario.

I. INTRODUCTION

Towed air gun arrays are used for marine geophysical imaging. The air guns produce a sound pulse by rapidly releasing compressed air into the water, thus generating an approximately spherical broadband wave, of short duration, centered on the air gun. An air gun array typically comprises several towed subarrays each containing several air guns. The air guns are suspended from floats. The subarrays are usually equispaced in the crossline direction and are placed at the same inline offset. The air guns are often, but not always, deployed all at the same nominal depth. Each subarray comprises a number of air guns or air gun clusters towed in a line. When fired simultaneously, the individual air gun pulses reinforce coherently in the direction perpendicular to the plane of the array to create a high-amplitude pulse in that direction [item 1) in the Appendix]. The high amplitudes of these pulses lead to concern about possible adverse effects on marine fauna [items 2) and 5) in the Appendix]. Computer models of air gun sources were originally developed for geophysical imaging applications [item 6) in the Appendix], and thus focused on accurate predictions only at relatively low frequencies (order of 100 Hz or less) [item 7) in the Appendix]. More recently, air gun source models have been combined with sound propagation models to estimate received sound pressure fields in water [items 8) and 10) in the Appendix], and comparisons with measurements have shown that at low frequencies they work well, but at high frequencies their predictions deviate from the measurements and from each other [item 11) in the Appendix].

The same or similar models are used to estimate the received field and possible effects on biota (NMFS) [item 12) in the Appendix]. Some animals are sensitive to high-frequency sound (10 kHz or above), and the accuracy of the air gun source models at such frequencies is uncertain. The need to check the accuracy of model predictions of the sound field radiated by air gun arrays led to the International Airgun Modelling Workshop (henceforth "the Workshop") in July 2016, in Dublin, Ireland [item 13) in the Appendix]. After the Workshop, the IEEE JOURNAL OF OCEANIC ENGINEERING invited contributions to a Special Issue on Verification and Validation of Air Gun Source Signature and Sound Propagation Models. Test scenarios were specified for the special issue [item 14) in the Appendix], closely based on the Workshop test scenarios [item 13) in the Appendix]. Participation in the special issue was open to all. Invitations were extended by the guest editors to specialist air gun signature modelers and to all participants in the Workshop, with contributions reviewed by the journal in the usual way. The purpose of this editorial is to introduce this special issue. A companion editorial [item 15) in the Appendix] describes the background, motivation, preparation for, and execution of the Workshop. This editorial comprises the following:

1) a description of the test scenarios that authors were invited (though not required) to consider [item 14) in the Appendix];
2) a summary of the specified scenarios (see Section II);
3) papers describing source waveform predictions (see Section III);
4) papers describing sound field predictions, in the form of sound pressure or sound particle acceleration or both (see Section IV);
5) concluding remarks (see Section V).

Digital Object Identifier 10.1109/JOE.2019.2913942

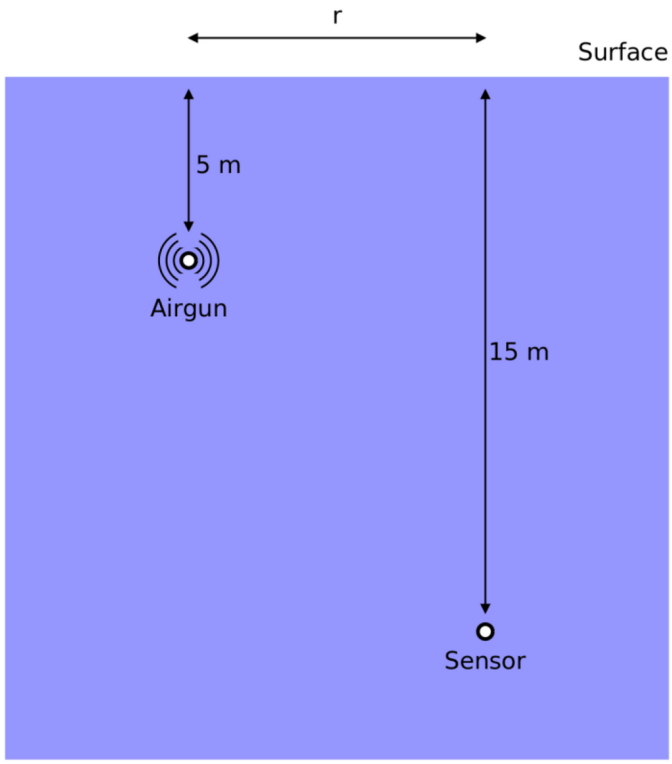

Fig. 1. Geometry for single air gun (source S1) at 5-m depth. Participants were requested to evaluate sound pressure $p(t)$ and sound particle acceleration $\boldsymbol{a}(t)$ at 15-m depth; with horizontal ranges r between 3 m and 30 km. See Ainslie *et al.* [item 14) in the Appendix] for details.

Acoustical terminology follows ISO 18405:2017 Underwater acoustics—Terminology [item 16) in the Appendix].

II. Summary of Test Scenarios

Three acoustic sources were specified, denoted by S1, S2, and S3. S1 is a single air gun of volume 2.5 L (155 in^3) and S2 is a horizontal line array of total volume of 21.5 L (1315 in^3) comprising six air guns, of which the third (designated S2G03) is the same air gun as S1. S3 is a large air gun array comprising three horizontal subarrays, with a total volume of 546 L (3333 in^3). The center subarray of S3 comprises the same air guns as S2 and nominally in the same positions. In all cases, the source depth is nominally 5 m and the chamber pressure is 13.79 MPa (2000 lbf/in^2). The properties of the three sources are fully described in Ainslie *et al.* [item 14) in the Appendix].

The source–receiver geometry for a single air gun is illustrated in Fig. 1. The horizontal range r was between 3 m and 30 km. In our editorial, we chose to compare model predictions from different authors at $r = 30$ m and 3000 m, with absorption in water switched off (problem 1 from [item 14) in the Appendix]).

III. Contributions Describing Source Waveforms

Three papers are included in the special issue that describe different implementations of computer models for calculating source signatures of seismic air guns. Notably, all three models employed some variant of spherical bubble theory to solve the equations of motion for an air gun bubble and predict its radiated source waveform (also known as its "notional signature"). While the different models included different physical effects in their equations of motion and employed different tuning parameters, they nonetheless followed the same general dynamical theory proposed by Ziolkowski [item 6) in the Appendix], augmented in one case [item 17) in the Appendix] with a stochastic spectrum model for high frequencies. The popularity of Ziolkowski's approach is no doubt a reflection of the fact that spherical bubble theory is well developed, and its predictions have been extensively verified against experimental data [item 18) in the Appendix]. For frequencies of interest to geophysical imaging, the bubble is small compared with the wavelength. Nonetheless, other computational methods do exist for calculating source signatures of air guns, such as scaling of recorded signatures [item 19) in the Appendix] and computational fluid dynamics [item 20) in the Appendix], which are not covered in this special issue and which may yet be of interest for future verification studies.

A. Source Waveform Papers

The article by Sertlek and Blacquière [item 21) in the Appendix] describes the Agora air gun model and applied this model to a detailed investigation of the effects of sea-surface roughness on measured waveforms of single air guns. Agora is the most recently developed of the three models and was also used to generate reference signatures for the Workshop [item 13) in the Appendix]. Using a three-dimensional scattering model, Sertlek and Blacquière demonstrate how sea-surface roughness affects measured sound pressure spectra for single air guns. By comparing model predictions with single-gun measurements from the Svein Vaage experiment [item 22) in the Appendix], Mattsson *et al.* show how observed variations in air gun spectra above 300 Hz may be explained by even moderate sea-surface conditions (i.e., sea state 2). Given that most extant air gun models are tuned using field calibration data, which suggests that some high-frequency differences between models may be attributable to the sea conditions under which different calibration data were obtained.

The article by MacGillivray [item 17) in the Appendix] describes the air gun array source model (AASM) and shows validation comparisons with experimental data. At low frequencies (below 800 Hz), an AASM employs a spherical bubble model, but at high frequencies (above 800 Hz), it uses a statistical model to predict the envelope of the initial peak of the single-gun signature. The statistical model is based on a principal component regression model of the single-gun spectrum and was derived from an analysis of the Svein Vaage data set. The statistical model also incorporates a stochastic component, which uses a Monte Carlo simulation to simulate shot-to-shot variability in the high-frequency single-gun spectrum. This type of variability is different from the variability due to sea-surface roughness described by Sertlek and Blacquière [item 21) in the Appendix] because it is related to measured variations in the direct-path signal, not the surface-reflected signal. As such, this stochastic component is conjectured to be related to anisotropy in the

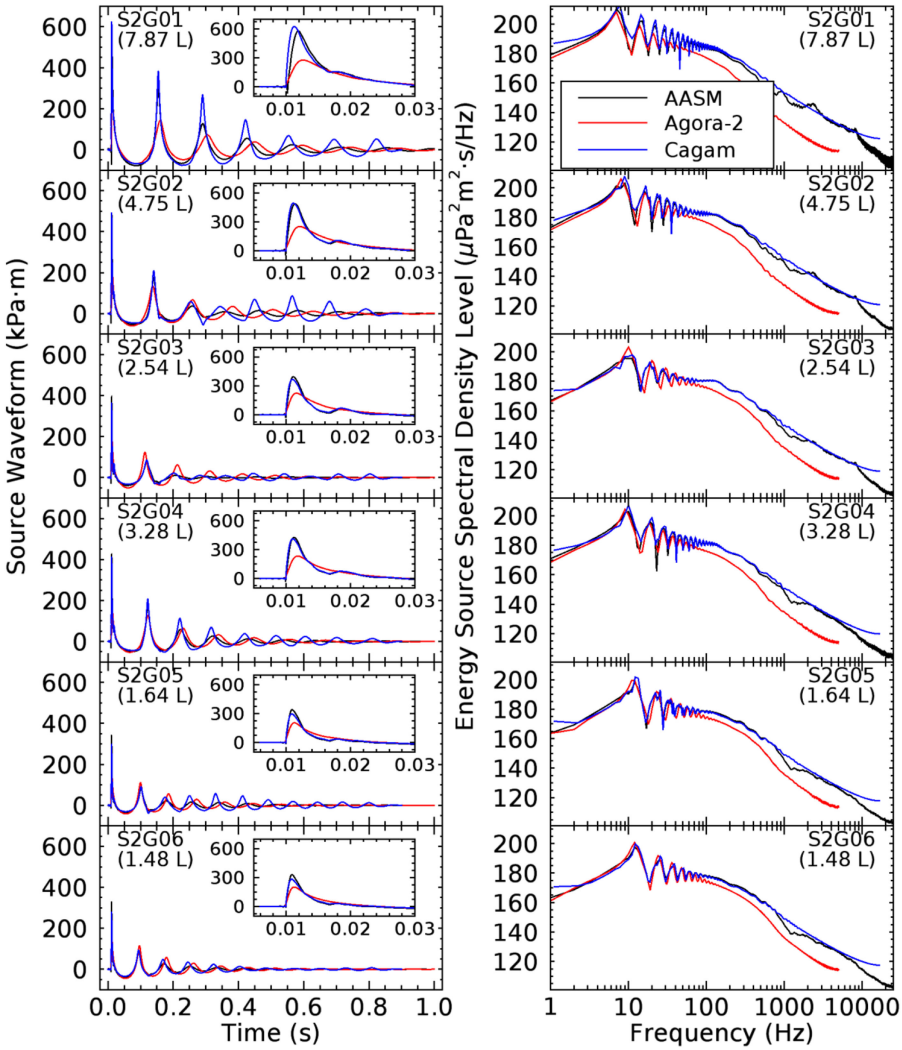

Fig. 2. Source S2 comparison of air gun source waveforms $s(t)$ (left) and the corresponding energy source spectral density levels [item 14) in the Appendix] (right) as computed by AASM, Agora 2, and Cagam. Source waveforms have been aligned in time so that the signal crosses 20 kPa · m at $t = 10$ ms. Insets on the left panels show the first 30 ms of the source waveform. Annotations indicated the air gun number from the problem description and the volume of the specified element.

shape of the air gun bubble (i.e., breaking of the spherical bubble assumption), though this remains to be confirmed experimentally.

The article by Duncan and Gavrilov [item 23) in the Appendix] describes the CMST air gun array model (Cagam) and shows validation comparisons of their model predictions with measurements. Cagam is based on a simplified bubble model (essentially a damped Rayleigh model), which incorporates fewer tuning parameters than the other models described in the special issue. The tradeoff of this simplified approach is that Cagam necessarily incorporates an amplitude scaling parameter that is used to match its output to reference signature data for a particular source. Such signatures originate either from established models (typically Nucleus [item 24) in the Appendix] or Gundalf [items 25) and 26) in the Appendix]) or from measurements. Nonetheless, the authors show that Cagam's predictions, suitably scaled, are in good agreement with single-gun measurements from the Svein Vaage experiment. Thus, this simplified method may present an attractive approach when reference signatures are available for the source of interest.

B. Comparison of Source Waveforms

Selected comparisons are described below for the signatures of source S2, in the form of source waveforms $s(t)$, of each of the six air guns in the line array and the surface-affected source waveform of the array. Source waveforms computed by the three source models are plotted side by side, for each individual air gun making up the array corresponding to source S2, to show how their predictions compare with each other (see Fig. 2). Observed differences at high frequencies (approximately above 100 Hz) are due to differences in the initial peaks (inset of Fig. 2), whereas the differences at low frequencies (approximately below 100 Hz) are due to differences in the bubble pulses. The bubble pulse spectra of the three models agree reasonably well, but the Agora 2 source waveforms (the difference between

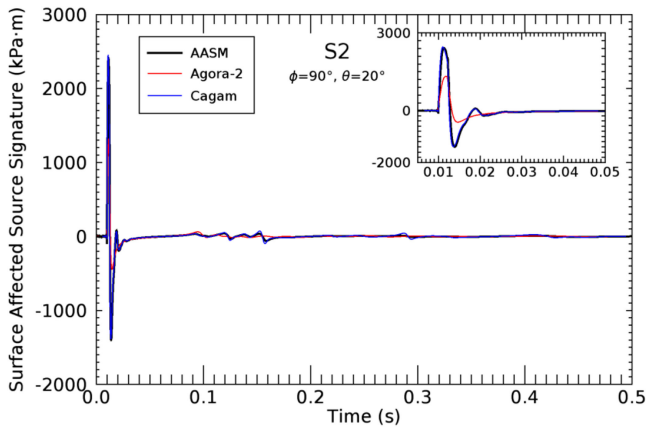

Fig. 3. Source S2 comparison of surface-affected source waveforms, as predicted by AASM, Agora 2, and Cagam, for the broadside direction, 20° below the horizontal (i.e., elevation angle $\theta = 20°$ and bearing angle$\varphi = 90°$). Each trace depicts the sums of the time-delayed source waveforms for the individual air guns in the array, plus their surface images, in the specified direction (often referred to as the "far-field signature" in reflection seismology).

Agora 1 and Agora 2 is explained in Ainslie *et al.* [item 14) in the Appendix]) have a lower high-frequency spectrum, due to the slower onset predicted by this model. The initial peaks predicted by Cagam and AASM are in much closer agreement, with the former model predicting slightly higher levels than the latter. Surface-affected source waveforms (i.e., far-field signatures) for the S2 array are plotted for 20° below the horizontal in the broadside direction for the three source models (see Fig. 3). Including the surface reflections (i.e., ghosts) in the far-field summation tends to suppress the bubble pulses; therefore, differences between the surface-affected source waveforms [item 16) in the Appendix] for the S2 array are due primarily to differences in the initial peaks predicted by the three models.

Overall, the agreement between the three models is best at low frequencies (as demonstrated at the Workshop [item 13) in the Appendix]) although two of the models (AASM and Cagam) also agree reasonably well at high frequencies. This agreement is notable given the marked differences in how these two models treat the port throttling that is responsible for the initial expansion of the air gun bubble. Indeed, implementations of the air gun port throttling physics are much more similar between AASM and Agora. This suggests that high-frequency differences between the three models are more related to differences in tuning data than to differences in the underlying physical models. For example, AASM was tuned against air gun signatures from the Svein Vaage data set [item 22) in the Appendix], whereas Agora 2 employed tuning parameters based on a data set for older air guns [item 27) in the Appendix]. Note that any model tuning procedure that is based on matching acoustical pressure or signal energy (e.g., as described in the article by Duncan and Gavrilov [item 23) in the Appendix]) will naturally tend to be weighted toward matching low frequencies (i.e., since this is where signal energy from air guns is concentrated). This may also help to explain why the three models diverge more at high frequency than at low frequency.

IV. Contributions Describing Sound Pressure and Acceleration Time Series

The challenges associated with modeling the acoustic time series of sound pressure and acceleration are significant. The greatest challenge to many numerical models is the large bandwidth (0–2500 Hz) and the high angles of propagation that must be supported at ranges nearer than 1 km in 50 m of water. The phase stability and bookkeeping requirements are also a challenge for computing the coherent field (time series) and derivatives for multiple sources. In this special issue, we have three papers in which the authors computed various acoustic values using the provided source time series from Agora [item 28) in the Appendix]. The test scenarios for this special issue [item 14) in the Appendix] are based on previous benchmark problems [items 29)–31) in the Appendix], using the classic Pekeris model, with isovelocity water, flat seafloor, and uniform fluid sediment. The extension of the previous work is to include a broadband source spectrum, the requirement for the coherent field for a set of arrays of sources (with different time series) including in the along-track (forward end fire) and cross-track (broadside) directions and the request for the computation of sound particle acceleration. In all, we compare six sound pressure time series results and three particle acceleration results using four different methods.

A. Propagation Papers

The paper by Küsel and Siderius [item 32) in the Appendix], presents the pressure time series for the single-gun air gun case for three very different modeling approaches. They solved the pressure time series to ranges of 3 km using a ray trace (RT) model called Bellhop [item 33) in the Appendix], a parabolic equation (PE) model called RAM [item 34) in the Appendix] and a wave number integration (WNI) method called OASP [item 35) in the Appendix]. Each of these models has different regions of validity and a different set of user skill sets required to produce reliable results. Before application to the Workshop scenarios, the RT and WNI models were tested against an exact image calculation for $p(t)$ in a fluid half-space. RT models are excellent for broadband time series (the ray arrival times are assumed to be independent of frequency). The PE solution is excellent for efficiently handling laterally invariant environments, but struggles with high angles (ray paths steeper than 85° from horizontal) and higher frequencies. The WNI solution is the closest to the mathematically exact solution for a problem in a laterally invariant environment.

The work in Prior *et al.* [item 36) in the Appendix] is a careful application of the method of images and a WNI model called Scooter [item 37) in the Appendix], with both a Hankel and a Fourier transform solution. They have computed both the sound pressure and sound particle acceleration time series, using high-precision coherent summations from the multiple sources and spatial derivatives of the field at the receiver. In principle, the method of images requires a new image for each surface or bottom multipath. However, because of approximations in applying the image method to bottom reflections, the authors choose to include only the direct path and its surface-reflected image,

thus providing a highly accurate reference for Scooter at short ranges only. For the same reason, they limit their predictions in their published paper to a maximum range of 30 m, showing that at these distances, the WNI method needs to replace the approximate Fourier transform with the full Hankel transform to maintain accuracy. Although the paper by Prior *et al.* [item 36) in the Appendix] presents results up to 30 m only, for the purposes of this editorial, the authors of that article made their predictions available up to 3000 m.

Heaney and Campbell [item 38) in the Appendix] present results using the PE model Peregrine, which is a C-language refactorization of RAM. There has been no change to the propagation physics from RAM, only to the environmental interface and the way that memory and CPU access are applied. Peregrine also internally computes the range and depth spacing required to support high angle propagation as a function of frequency. Heaney and Campbell were able to use the code to improve phase accuracy and to output the acoustic field on the computational grid, which permitted the computation of the sound particle acceleration. In particular, the computational grid was required to land exactly on the receiver. The sound pressure and particle acceleration are provided for each of the three sources (single source, single line array, and triple line array) at all of the specified ranges and bearings, with the exception of the 3-m range. This was not computed because the PE as a range marching algorithm struggles at very high angles. This paper addresses all of the source arrays requested in the problem set definition [item 14) in the Appendix]. In Section IV of [item (38) in the Appendix], the authors apply the model for the S3 (triple line array) source array transmitting in the Gulf of Mexico. The pressure time series is computed out to a range of 30 km (requiring phase accuracy across the full band) and the incoherent sound exposure level is computed out to 1000 km (requiring phase accuracy across the multiple source air guns).

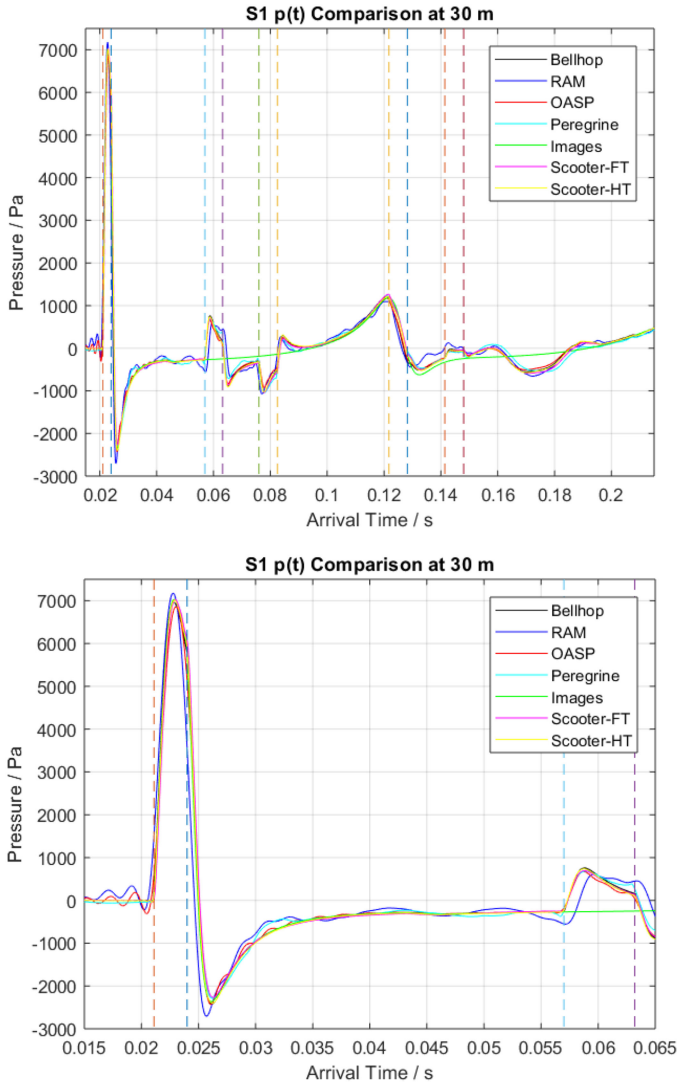

Fig. 4. Source S1 (a single air gun, identical to S2G03) sound pressure time series $p(t)$ at 30-m range. The lower graph zooms in on the direct path and first bottom reflection, with corresponding surface images.

B. Comparison of Sound Pressure and Particle Acceleration

This section includes selected comparisons of the sound pressure $p(t)$ and the horizontal component of sound particle acceleration $a_r(t)$ for source S1. Source S1 is the same air gun as the third air gun in source S2. In all cases, the predictions are made using the Agora 2 source waveforms provided by the organizers to the Workshop participants [item 14) and 15) in the Appendix], which means that any differences are caused by differences in the propagation modeling or in the interface between the signature and propagation models.

We now compare the pressure time series for two ranges for the S1 case (the third air gun in the S2 array, "S2G03"—see Ainslie *et al.* [item 14) in the Appendix]). All six models' results are available at 30 m (see Fig. 4), which is an interesting range because there is still a lot of high angle propagation, but also a significant amount of bottom interaction. The predictions of Bellhop (RT), Peregrine (PE), and two WNI models (OASP and Scooter) are so close together that one can hardly distinguish the individual curves. For Scooter, calculations were provided using both the default Fourier transform method (Scooter-FT) and the more accurate Hankel transform (Scooter-HT). For this geometry, the difference is small, and subsequent figures use only the Fourier transform (Scooter).

Agreement of this caliber between RT, PE, and WNI methods provides a strong indication that all four curves are accurate—the chances of all being in error by the same amount is very small. A second PE model (RAM) predicts the main features while differing in detail. The method of images omits bottom-reflected paths by design. The vertical dashed lines in Figs. 4 and 6 show expected arrival times for the first ten multipaths, the first four being the direct path (21 ms, red) and its surface image (24 ms, blue) and the first bottom reflection (57 ms, cyan) and its image (63 ms, magenta).

The peak sound pressure at this receiver position (31.6 m from the air gun) using Agora 2 is 7 kPa (corresponding to a peak sound pressure level with reference to 1 μPa^2, abbreviated L_{pk}, of 197 dB) for the primary peak at 23 ms and 1.1 kPa (L_{pk} of 181 dB) at 122 ms for the secondary peak (sometimes known as a "bubble pulse" [item 1) in the Appendix]). The agreement

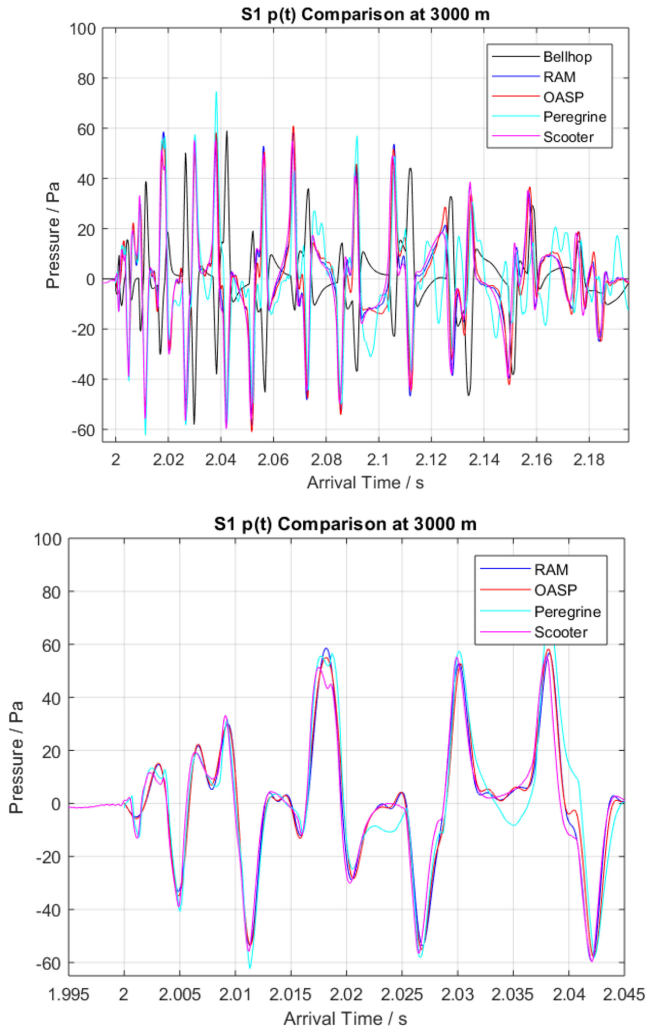

Fig. 5. Source S1 (a single air gun, identical to S2G03) sound pressure time series $p(t)$ at 3000-m range. The lower graph zooms in on the direct path and first bottom reflection, with corresponding surface images. The detailed structure predicted by Bellhop is different from that of the other models, and Bellhop is therefore omitted from the lower graph to avoid distraction from the small differences between the other four solutions.

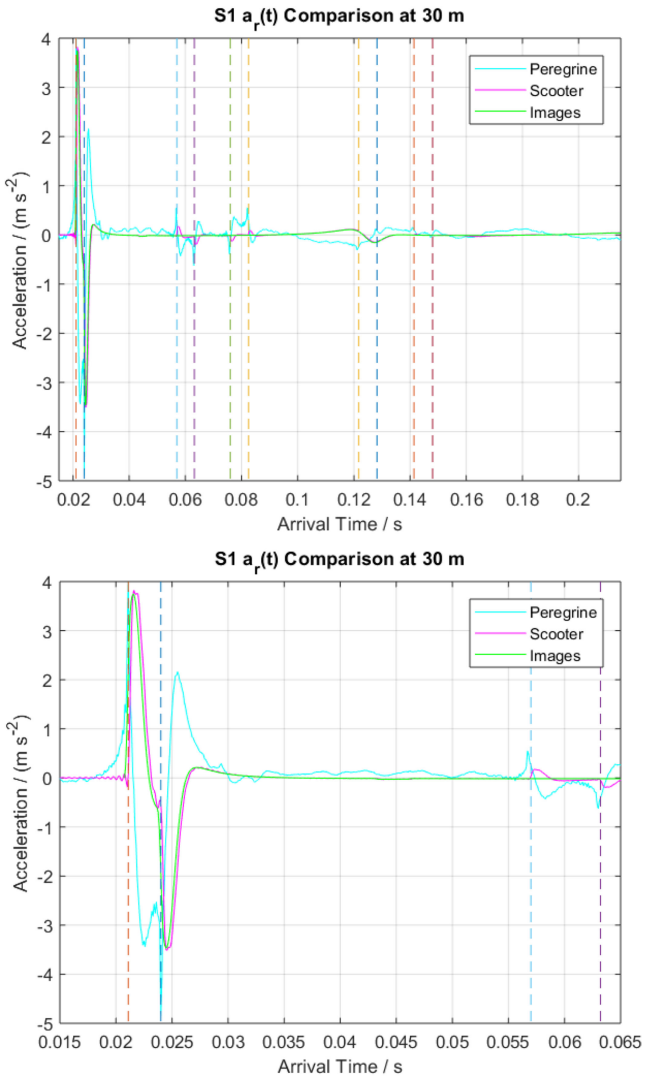

Fig. 6. Source S1 (Gun 3) horizontal sound particle acceleration time series $a_r(t)$ at 30-m range. The lower graph zooms in on the direct path and first bottom reflection, with corresponding surface images.

between all six models (and three independent groups of modelers) is a remarkable testimony to the model maturity and the modelers' skill.

However, the same calculations using AASM or Cagam would have increased the predicted peak sound pressure to about 12.5 Pa (L_{pk} of 202 dB). At short range, the main source of uncertainty in the peak sound pressure arises from the choice of source signature model.

The pressure time series at 3000 m are presented for five out of the six models (see Fig. 5). The peak sound pressure using the Agora 2 signature for source S1 is 60 Pa (L_{pk} of 156 dB). Peregrine shows similar features, with higher frequency oscillations not seen in the output of the other models.

The acceleration was provided by two authors at 30-m range. In Fig. 6, we compare the Prior *et al.* [item 36) in the Appendix] acceleration (horizontal component) computed using the method of images and the WNI model Scooter, with the Heaney and Campbell result using the PE. Both models computed the acceleration via the spatial derivative of the sound pressure. With only three curves, it is harder to make conclusive statements for $p(t)$, but the close agreement between Scooter and images for the primary peak leads to the likely conclusion that Scooter is providing an accurate solution. The horizontal component of the sound particle acceleration at this receiver position (31.6 m from the source) has a peak magnitude of 3.8 m·s^{-2}.

V. Concluding Remarks

The main purpose of this special issue is to consolidate the results presented at the Workshop. The focus of the Workshop was on verification, meaning comparison between model predictions for specified scenarios. Predictions of source waveform $s(t)$ from the air gun models AASM, Agora 2, and Cagam were compared. The three models predict similar features, with the main differences appearing in the height and rise time of the

primary peak, leading to corresponding differences in the energy spectral density. When results for sound pressure $p(t)$ were compared for fixed $s(t)$, we find remarkable consistency between $p(t)$ model predictions from the PE, WNI, RT, and image methods, for the two ranges considered (30 and 3000 m).

We conclude that the consolidation of the verification step is sufficiently mature to merit progression to a validation study (comparison with measurements). We believe that suitable data sets exist, both for individual air guns or clusters [item 22) in the Appendix] and full air gun arrays [item 11) in the Appendix]. Furthermore, verification steps could include consideration of a rough sea surface, a more realistic seabed or nonlinear propagation in the high intensity region near an air gun.

Significant progress has also been made with sound particle acceleration, especially by comparing wave number integration and image solutions (see Fig. 6). These promising results need further verification by independent comparison with other methods.

Acknowledgment

The Guest Editors would like to thank G. Blacquière, R. L. Campbell, A. J. Duncan, A. N. Gavrilov, E. T. Küsel, R. M. Laws, M. K. Prior, H. Ö. Sertlek, and M. Siderius for contributing to this special issue. They would also like to thank R. P. A. Dekeling and M. B. Halvorsen for co-organizing the workshop and N. R. Chapman for his patience and inspiration.

M. A. Ainslie, *Guest Editor*
JASCO Applied Sciences (Deutschland) GmbH
65760 Eschborn, Germany.

K. D. Heaney, *Guest Editor*
Applied Ocean Sciences, LLC
Fairfax Station, VA 22039 USA.

A. O. MacGillivray, *Guest Editor*
JASCO Applied Sciences (Canada), Ltd.,
Victoria, BC V8Z 7X8, Canada.

Appendix
Related Work

1) B. Dragoset, "Introduction to air guns and air-gun arrays," *Leading Edge,* vol. 19, no. 8, pp. 892–897, 2000.
2) B. L. Southall *et al.*, "Marine mammal noise exposure criteria: Initial scientific recommendations," *Aquatic Mammals,* vol. 33, no. 4, pp. 411–521, 2007.
3) H. Slabbekoorn, N. Bouton, I. van Opzeeland, A. Coers, C. Ten Cate, and A. N. Popper, "A noisy spring: The impact of globally rising underwater sound levels on fish," *Trends Ecol. Evol.,* vol. 25, no. 7, pp. 419–427, 2010.
4) A. N. Popper *et al.*, *Sound Exposure Guidelines for Fishes and Sea Turtles: A Technical Report Prepared by ANSI-Accredited Standards Committee S3/SC1 and Registered With ANSI* (ASA S3/SC1.4 TR-2014. SpringerBriefs in Oceanography). New York, NY, USA: Springer, 2014.
5) R. D. McCauley, R. D. Day, K. M. Swadling, Q. P. Fitzgibbon, R. A. Watson, and J. M. Semmens, "Widely used marine seismic survey air gun operations negatively impact zooplankton," *Nature Ecol. Evol.,* vol. 1, no. 7, pp. 1–8, 2017.
6) A. Ziolkowski, "A method for calculating the output pressure waveform from an air gun," *Geophys. J. Roy. Astron. Soc.,* vol. 21, no. 2, pp. 137–161, 1970.
7) J. F. Wisløff, D. Barker, S. Hegna, A. Goertz, F. Pesnel, and D. Richelmi, "Calibrated airgun source modeling to estimate broadband marine source signatures," in *Proc. SEG Tech. Program Expanded Abstr.,* 2014, pp. 238–242.
8) A. O. MacGillivray, "An Acoustic modelling study of seismic airgun noise in Queen Charlotte Basin," M.Sc. thesis, School Earth Ocean Sci., Univ. Victoria, Victoria, BC, Canada, 2006.
9) S. L. DeRuiter, P. L. Tyack, Y.-T. Lin, A. E. Newhall, J. F. Lynch, and P. J. O. Miller, "Modeling acoustic propagation of airgun array pulses recorded on tagged sperm whales (*Physeter macrocephalus*)," *J. Acoust. Soc. Amer.,* vol. 120, no. 6, pp. 4100–4114, 2006.
10) B. Khodabandeloo, M. Landrø, and A. Hanssen, "Acoustic generation of underwater cavities—Comparing modeled and measured acoustic signals generated by seismic air gun arrays," *J. Acoust. Soc. Amer.,* vol. 141, no. 4, pp. 2661–2672, 2017.
11) A. M. Tashmukhambetov, G. E. Ioup, J. W. Ioup, N. A. Sidorovskaia, and J. J. Newcomb, "Three-dimensional seismic array characterization study: Experiment and modeling," *J. Acoust. Soc. Amer.,* vol. 123, no. 6, pp. 4094–4108, 2008.
12) Office of Protected Resources, National Marine Fisheries Service, "2018 revision to: Technical guidance for assessing the effects of anthropogenic sound on marine mammal hearing (version 2.0): Underwater thresholds for onset of permanent and temporary threshold shifts," U.S. Dept. Commerce, Nat. Ocean. Atmos. Admin., Silver Spring, MD, USA, NOAA Tech. Memorandum NMFS-OPR-59, 2018. [Online] Available: https://www.fisheries.noaa.gov/webdam/download/75962998
13) M. A. Ainslie *et al.*, "Verification of airgun sound field models for environmental impact assessment," *Proc. Meetings Acoust.,* vol. 27, no. 1, 2006, Art. no. 070018.
14) M. A. Ainslie, R. M. Laws, and H. Ö. Sertlek, "International Airgun Modeling Workshop: Validation of source signature and sound propagation models—Dublin (Ireland), July 16, 2016—Problem description," *IEEE J. Ocean. Eng.*, vol. 44, no. 3, pp. 565–574, Jul. 2019.
15) M. B. Halvorsen, M. A. Ainslie, and R. P. A. Dekeling, "Editorial: The International Airgun Modelling Workshop," *IEEE J. Ocean. Eng.,* vol. 44, no. 3, pp. 560–564, 2019.
16) *Underwater Acoustics—Terminology*, ISO 18405:2017, Apr. 2017.

17) A. O. MacGillivray, "An airgun array source model accounting for high-frequency sound emissions during firing—Solutions to the IAMW source test cases," *IEEE J. Ocean. Eng.,* vol. 44, no. 3, pp. 582–588, Jul. 2019, doi: 10.1109/JOE.2018.2853199.
18) A. Prosperetti and A. Lezzi, "Bubble dynamics in a compressible liquid. Part 1. First-order theory," *J. Fluid Mech.,* vol. 168, pp. 457–478, 1986.
19) S. Vaage and B. Ursin, "Computation of signatures of linear airgun arrays," *Geophys. Prospecting,* vol. 35, no. 3, pp. 281–287, 1987.
20) D. Gerez, H. Groenaas, O. Pramm Larsen, M. Wolfstirn, and M. Padula, "Controlling air-gun output to optimize seismic content while reducing unnecessary high-frequency emissions," in *Proc. SEG Tech. Program Expanded Abstr.*, 2015, pp. 154–158.
21) H. Ö. Sertlek and G. Blacquière, "Effects of the rough sea surface on the signature of a single airgun," *IEEE J. Ocean. Eng.,* vol. 44, no. 3, pp. 575–581, Jul. 2019, doi: 10.1109/JOE.2018.2890464.
22) A. Mattsson, G. Parkes, and D. Hedgeland, "Svein vaage broadband air gun study," in *The Effects of Noise on Aquatic Life*, A. N. Popper and A. D. Hawkins, Eds. New York, NY, USA: Springer, 2012, pp. 469–471.
23) A. J. Duncan and A. N. Gavrilov, "The CMST airgun array model—A simple approach to modelling the underwater sound output from seismic airgun arrays," *IEEE J. Ocean. Eng.,* vol. 44, no. 3, pp. 589–597, Jul. 2019, doi: 10.1109/JOE.2019.2899134.
24) A. Goertz, J. F. Wisløff, F. Drossaert, and J. Ali, "Environmental source modelling to mitigate impact on marine life," *First Break,* vol. 31, no. 11, pp. 59–64, 2013.
25) R. M. Laws, L. Hatton, and M. Haartsen, "Computer modeling of clustered airguns," *First Break,* vol. 8, no. 9, pp. 331–338, 1990.
26) R. M. Laws, "The interaction of marine seismic sources," Ph.D. dissertation, Dept. Roy. Sch. Mines, Imperial College London, London, U.K., 1991.
27) R. G. Racca and J. A. Scrimger, "Underwater acoustic source characteristics of air and water guns," JASCO Res., Ltd., Victoria, BC, Canada, Contract 06SB 97708-5- 7055, 1986.
28) H. Ö. Sertlek and M. A. Ainslie, "Airgun source model (Agora): Its application for seismic surveys sound maps in the Dutch North Sea," in *Proc. Conf. Proc. UAC*, Crete, Greece, 2015.
29) J. S. Perkins and E. I. Thorsos, "Overview of the reverberation modeling workshops," *J. Acoust. Soc. Amer.,* vol. 122, no. 5, pp. 3074–3074, 2007.
30) J. S. Perkins and E. I. Thorsos, "Update on the reverberation modeling workshops," *J. Acoust. Soc. Amer.,* vol. 126, no. 4, pp. 2208–2208, 2009.
31) M. A. Ainslie, "Editorial: Validation of sonar performance assessment tools," in *Validation of Sonar Performance Assessment Tools: In Memory of David E Weston*, M. A. Ainslie, Ed. Cambridge, U.K.: Clare Coll., Univ. Cambridge, Apr. 2010, pp. 2–6.
32) E. T. Küsel and M. Siderius, "Comparison of propagation models for the characterization of sound pressure fields," *IEEE J. Ocean. Eng.,* vol. 44, no. 3, pp. 598–610, Jul. 2019, doi: 10.1109/JOE.2018.2884107.
33) M. B. Porter and H. P. Bucker, "Gaussian beam tracing for computing ocean acoustic fields," *J. Acoust. Soc. Amer.,* vol. 82, no. 4, pp. 1349–1359, 1987.
34) M. D. Collins, "A split-step Padé solution for the parabolic equation method," *J. Acoust. Soc. Amer.,* vol. 93, no. 4, pp. 1736–1742, 1993.
35) H. Schmidt and G. Tango, "Efficient global matrix approach to the computation of synthetic seismograms," *Geophys. J. Int.,* vol. 84, no. 2, pp. 331–359, 1986.
36) M. K. Prior, A. J. Duncan, H. Ö. Sertlek, and M. A. Ainslie "Modeling acoustical pressure and particle acceleration close to marine seismic airguns and airgun arrays," *IEEE J. Ocean. Eng.,* vol. 44, no. 3, pp. 611–620, Jul. 2019, doi: 10.1109/JOE.2019.2891873.
37) M. B. Porter, *Acoustics Toolbox*, Mar. 2019. [Online]. Available: http://oalib.hlsresearch.com/FFP/index.html
38) K. D. Heaney and R. L. Campbell, "Parabolic equation modeling of a seismic airgun array," *IEEE J. Ocean. Eng.*, vol. 44, no. 3, pp. 621–632, Jul. 2019, doi: 10.1109/JOE.2019.2912060.

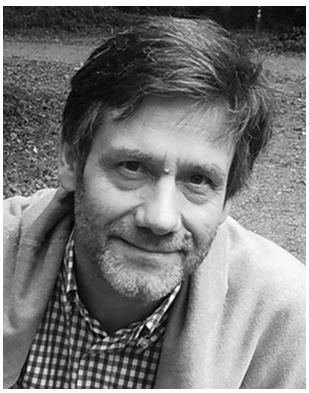

Michael A. Ainslie received the B.Sc. degree in physics from the Imperial College London, London, U.K., in 1981, the M.Sc. degree in mathematics from the University of Cambridge, Cambridge, U.K., in 2011, and the Ph.D. degree in seabed acoustics from the University of Southampton, Southampton, U.K., in 1991.

He is currently a Senior Scientist with JASCO Applied Sciences, Eschborn, Germany, and a Visiting Professor with the Institute of Sound and Vibration Research, University of Southampton. He is the author of the book *Principles of Sonar Performance Modeling* (New York, NY, USA: Springer-Verlag, 2010). He is a Convener of the ISO working group responsible for the development of ISO 18405:2017 Underwater acoustics—Terminology, the Co-Chair for the Standardization working group of the International Quiet Ocean Experiment (iqoe.org), and a Project Leader for the ongoing revision of ISO 80000-8:2007 Quantities and units—Acoustics. His research interests include sonar performance modeling and effects of sound on aquatic life.

Dr. Ainslie is a Fellow of the Acoustical Society of America and the U.K. Institute of Acoustics.

Kevin D. Heaney received the B.S. degree in physics (*cum laude*) from the University of California Santa Barbara, Santa Barbara, CA, USA, in 1987, the M.S. degree in physics from the University of Maryland, College Park, MD, USA, in 2000, and the Ph.D. degree in applied ocean sciences from the Scripps Institution of Oceanography, University of California at San Diego, La Jolla, CA, USA, in 1997.

He has extensive experience in ocean acoustic propagation and modeling, optimal oceanographic sampling and data assimilation, geoacoustic inversion, adaptive sonar signal processing, and data analysis. He has worked on a variety programs, including long-range ocean acoustic tomography, geoacoustic inversion and rapid environmental characterization, and effects of internal waves on signal coherence. He has successfully transitioned algorithms to NAVOCEANO, NAVSEA, and CNMOC. He also has significant experience in adaptive signal processing from both modeling and experimental perspectives.

Alexander O. MacGillivray received the B.Sc. (honors) degree in physics and the M.Sc. degree in earth and ocean sciences from the University of Victoria, Victoria, BC, Canada, in 2000 and 2006, respectively.

He is a Senior Scientist and a Project Manager with JASCO Applied Sciences, Victoria, BC, Canada, where he has been employed since 2001. He is the primary author of JASCO's Airgun Array Source Model (AASM). His research interests include computational methods for predicting underwater noise, underwater ambient noise measurement, and the environmental effects of noise on marine life.